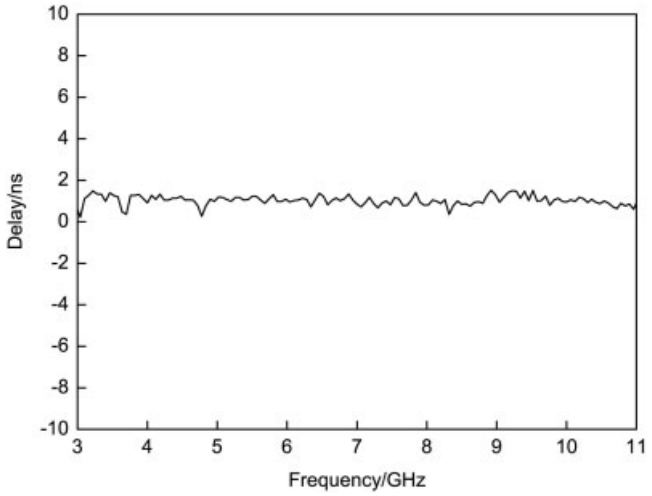

Figure 8 Measured group delay

that the patterns in *E*-plane and *H*-plane are approximately omni-directional over the entire operating bandwidth and suits UWB application. Figure 6 shows the measured peak gain of the proposed antenna. It is evident that the gain is relatively flat and change between about 4.78 to 7.89 dB.

Since UWB systems use short pulses to transmit signals, it is crucial to study the transfer function for evaluating the proposed antenna's performance and designing transmitted pulse signals. In this article a pair of proposed antennas are used as the transmitting and receiving antennas. Considering the antenna system as a two-port network, the transmission scattering parameter *S*21 which indicates the transfer function is measured by using an HP8722ES Vector network analyzer. For the measurement, the distance between the two antennas is 10 cm.

The measured parameter *S*21 and group delay are shown in Figures 7 and 8. It can be seen that the magnitude of *S*21 is relatively flat and the phase is nearly linear in the operation band. The group delay variation is less than 1.5 ns in this bandwidth. The measured results show that the group delay of the antenna system corresponds well to the magnitude of the transfer function. So it proves that the antenna has good time-domain characteristics for UWB applications.

4. CONCLUSION

A printed dipole antenna of double-side rectangular patch for UWB communications is proposed and investigated. The measured return loss less than −10 dB completely covers the UWB range of 3.1–10.6 GHz. The measured gains are relatively flat and change from 4.78 to 7.89 dB and the radiation patterns are approximately omni-directional within the UWB bandwidth. Besides, the proposed antenna has good time-domain characteristics for UWB applications.

ACKNOWLEDGMENT

This work was supported by the Shanghai Leading Academic Discipline Project (No. T102).

REFERENCES

1. H.G. Schantz, A brief history of UWB antennas, IEEE Aerosp Electron Syst Mag 19 (2004), 22–26.
2. J.I. Kim, B.M. Lee, and Y.J. Yoon, Wideband printed dipole antenna for multiple wireless services, Radio and Wireless Conference 2001, Waltham, MA, USA, 2001, pp. 153–156.
3. B.M. Lee, J.I. Kim, Y.J. Yoon, and J.I. Choi, Wideband printed fat dipole with folded balun, JINA (International Symposium on Antennas) 2002, Nice, France, 2002, pp. 259–262.
4. J.I. Kim, Y.J. Yoon, and C.S. Pyo, Wideband printed fat dipole fed by tapered microstrip balun, IEEE Antenna Propagat Soc Int Symp 3 (2003), 32–35.
5. K.H. Kim, S.B. Cho, Y.J. Park, and H.G. Park, Novel planar ultra-wideband stepped-fat dipole antenna, Proc IEEE Conf Ultra Wideband Systems and Technologies, Reston, VA, 2003, pp. 508–512.
6. X.H. Wu and Z.N. Chen, Comparison of planar dipoles in UWB applications, IEEE Trans Antennas Propagat 53 (2005), 1973–1981.
7. E. Lule, T. Babi, and K. Siwiak, Diamond dipole antenna for ultra-wideband communications, Microwave Opt Technol Lett 46 (2005), 536–538.
8. Y.M. Lu, X.X. Yang, and G.X. Zheng, Analysis on a novel ultra-wide bandwidth antenna of double-printed circular disc, Microwave Opt Technol Lett 49 (2007), 311–313.

SPHERICAL REPRESENTATION OF OMNIPOTENT SMITH CHART

Yongle Wu,[1] Haiyu Huang,[2] Yuanan Liu,[1] Zehua Gao[1]
[1] School of Telecommunication Engineering, Beijing University of Posts and Telecommunications, P.O. Box 171, Beijing 100876, China; Corresponding author: wuyongle138@gmail.com
[2] Department of Electrical Engineering, Columbia University, New York 10027, NY

Received 23 January 2008

ABSTRACT: *In this article, A spherical representation of omnipotent Smith chart (OSC) for lossy nonreciprocal transmission lines (LNTLs) is presented. Such representation is an extension of OSC to deeply understand the general transmission lines with not only positive parameters but also negative ones. The spherical OSC has great potential in the application of RF systems which involve active devices. The mathematical expressions and the three-dimensional (3D) graphics of the representation are showed in detail.* © 2008 Wiley Periodicals, Inc.
Microwave Opt Technol Lett 50: 2452–2455, 2008; Published online in Wiley InterScience (www.interscience.wiley.com). DOI 10.1002/mop.23689

Key words: *spherical representation; omnipotent Smith chart; active RF devices*

1. INTRODUCTION

As the coming out of omnipotent Smith chart (OSC), solutions of lossy nonreciprocal transmission lines (LNTLs) problems become possible with the help of this novel graphical tool [1, 2]. To the author's best knowledge, OSC is now one of the most general graphical tools compared to other kinds of improved Smith charts which have been reported [3–7]. However, an initial drawback always lies in all those Smith charts including OSC, which is the neglect of cases with negative impedance. Although efforts have been made to design an extended OSC specifically to meet the requirement of negative impedance analysis [2], it was at the sacrifice of the usage for positive impedance. What engineers mostly call for is a single graphical tool capable of illustrating RF devices containing lossy, nonreciprocal devices with both active and passive components.

This article contains supplementary material available via the Internet at http://www.interscience.wiley.com/jpages/1098-2760/suppmat.

Fortunately, Zelley [8] provided that the two-dimensional (2D) standard Smith chart can be converted into three-dimensional (3D) space. Getting the hint form this idea, we establish our own 3D coordinate system, which is simpler than its counterpart to help understand the negative impedances. Furthermore, knowing that the standard Smith chart is a special case of OSC [1], the spherical representation of OSC, which combines together cases with positive and negative parameters, have become a possible way to overcome this drawback.

2. MATHEMATICAL EXPRESSION OF OSC

In this section, the instruction of OSC is reviewed briefly [1]. In LNTLs of Figure 1, the characteristic impedances Z_0^+ and Z_0^- in the forward and reverse directions are defined as follows:

$$Z_0^+ = |Z_0|e^{j\theta_1},\ Z_0^- = \frac{1}{p}|Z_0|e^{j\theta_2} \tag{1}$$

where $|Z_0|$ and θ_1 are the magnitude and the argument of Z_0^+ , and p and θ_2 are the magnitude ratio coefficient and the argument of Z_0^- [1].

To find out the OSC mathematic expression, the original equations can be written as follows:

$$z = r + jx = \frac{1+\Gamma}{e^{-j\theta_1} - pe^{-j\theta_2}\Gamma},\ \Gamma = \Gamma_r + j\Gamma_i,\ y = 1/z = g + jb \tag{2}$$

From (1 and 2), the mathematic equations about OSC can be written as follows:

$$\left(\Gamma_r - \frac{pr\cos(\theta_1-\theta_2) - 0.5p\cos\theta_2 + 0.5\cos\theta_1}{p^2r + p\cos\theta_2}\right)^2 + \left(\Gamma_i - \frac{pr\sin(\theta_2-\theta_1) - 0.5p\sin\theta_2 - 0.5\sin\theta_1}{p^2r + p\cos\theta_2}\right)^2 = \frac{p^2+1+2p\cos(\theta_2-\theta_1)}{4(p^2r + p\cos\theta_2)^2} \tag{3}$$

$$\left(\Gamma_r - \frac{px\cos(\theta_1-\theta_2) - 0.5p\sin\theta_2 + 0.5\sin\theta_1}{p^2x + p\sin\theta_2}\right)^2 + \left(\Gamma_i - \frac{px\sin(\theta_2-\theta_1) + 0.5p\cos\theta_2 + 0.5\cos\theta_1}{p^2x + p\sin\theta_2}\right)^2 = \frac{p^2+1+2p\cos(\theta_2-\theta_1)}{4(p^2x + p\sin\theta_2)^2} \tag{4}$$

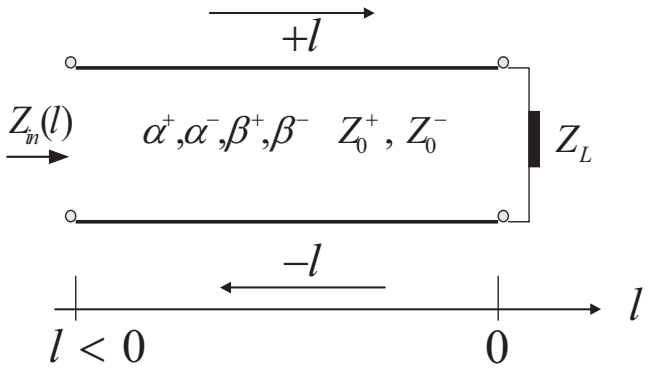

Figure 1 Generalized model of LNTLs [1]

$$\left(\Gamma_r + \frac{g - 0.5\cos\theta_1 + 0.5p\cos\theta_2}{g + p\cos\theta_2}\right)^2 + \left(\Gamma_i + \frac{\sin\theta_1 + p\sin\theta_2}{2g + 2p\cos\theta_2}\right)^2 = \frac{p^2+1+2p\cos(\theta_2-\theta_1)}{4(g + p\cos\theta_2)^2} \tag{5}$$

$$\left(\Gamma_r + \frac{b + 0.5\sin\theta_1 - 0.5p\sin\theta_2}{b - p\sin\theta_2}\right)^2 + \left(\Gamma_i + \frac{\cos\theta_1 + p\cos\theta_2}{2b - 2p\sin\theta_2}\right)^2 = \frac{p^2+1+2p\cos(\theta_2-\theta_1)}{4(b - p\sin\theta_2)^2} \tag{6}$$

Their plots in 2D are showed in the figures of [1, 2]. Obviously, the constant resistance circle of OSC in [1] cannot be presented completely when $r < 0$. In a similar case, the constant resistance circle of OSC with active parameters in [2] cannot be presented completely when $r > 0$. To overcome this drawback, a spherical presentation along with some improvement of normalization is presented in the following section.

3. SPHERICAL REPRESENTATION OF OSC

We establish the spherical space by adding the third dimension Γ_z in which the coordinate system is defined by obtaining the following equation:

$$\left(\frac{\Gamma_r}{|\Gamma|_{\max}}\right)^2 + \left(\frac{\Gamma_i}{|\Gamma|_{\max}}\right)^2 + \left(\frac{\Gamma_z}{|\Gamma|_{\max}}\right)^2 = 1 \tag{7}$$

where $|\Gamma|_{max}$ is the largest reflection coefficient amplitude in the case when $r = 0$ or $g = 0$, which is as follows:

$$|\Gamma|_{\max} = \frac{\sqrt{p^2+1-2p\cos(\theta_2+\theta_1)} + \sqrt{p^2+1+2p\cos(\theta_2-\theta_1)}}{2|p\cos\theta_2|} \tag{8}$$

To plot the OSC in 3D, we use the $\frac{\Gamma}{|\Gamma|_{\max}}$ as the normalized value.

When the constant resistance circles are outside of the $r = 0$ circle (the same to conductance circles), they are put on the lower hemisphere ($\Gamma_z < 0$) and the characteristic impedance must be negated in order to normalize the load impedance. Note that for spherical OSC, the resistance circle r is not necessarily positive even if it is in the upper hemisphere and it depends on other three parameters θ_1, θ_2, p. For example, for the OSC with active parameters [2], the resistance circle r is negative in the upper hemisphere. Details of those characteristics can be seen from examples provided in the next section.

4. TYPICAL EXAMPLES OF SPHERICAL REPRESENTATION

In this section, some typical examples of spherical OSC are illustrated.

While $\Gamma_z = 0$, the OSC degenerates to the famous Smith chart, which is called the standard Smith chart. Figure 2 shows the spherical standard Smith chart, which is different from the one in [8]. Obviously, the constant reflection coefficient circles are purely the circles' shape. A and B are the matching point and open-circuit point, respectively, on the sphere surface, C is the open-circuit point B which is mapped to the $\theta_2 = -\theta_1, p = 1$ plane. The equator is the $r = 0$ constant resistance circle and all the points with the positive resistance are located on the upper hemisphere. All the negative constant impedance circles are at the lower hemisphere, not as those in the plane which spread to infinite. The

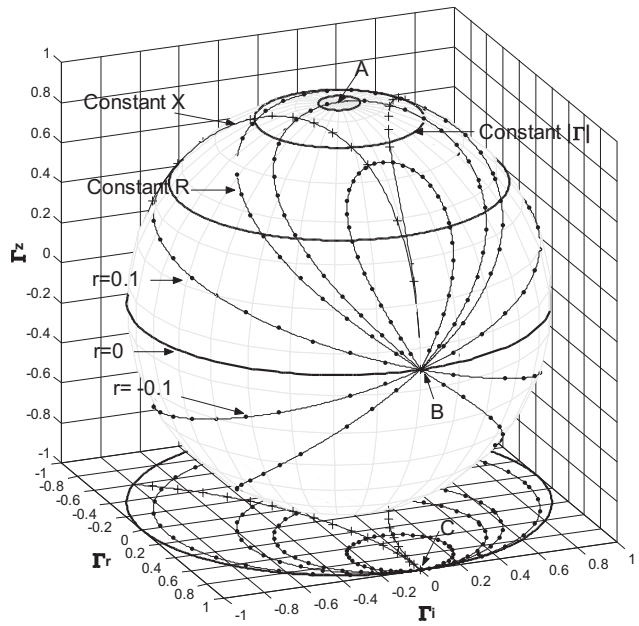

Figure 2 Standard Smith chart spherical representation ($|\Gamma|_{\max} = 1$)

exact locations of constant impedance circles for $r = 0.1$ and $r = -0.1$ are provided and, only $r = 0$ circle (equator) keeps its original position and shape as in the plane coordinate system.

While $\Gamma_r - \Gamma_x$, the OSC degenerates to the generalized Smith chart (called T-Chart) [4, 7]. Figure 3 shows the spherical T-chart. The points A, B, and C have the same physical characteristics with Figure 2, but it rotates by some angle. For comparison, the $r = 0.1$ and $r = -0.1$ constant impedance circles are also showed; it can be seen that they are also after rotation of standard Smith chart in the $\Gamma_r - \Gamma_x$ plane. Moreover, the chart changes in shape, actually the constant impedance with the same value have different size and shape, which can be seen in Figure 3.

Figure 4 shows the spherical OSC, which is considered as the most general case for LNTLs, Point A keeps unmoved, but B and

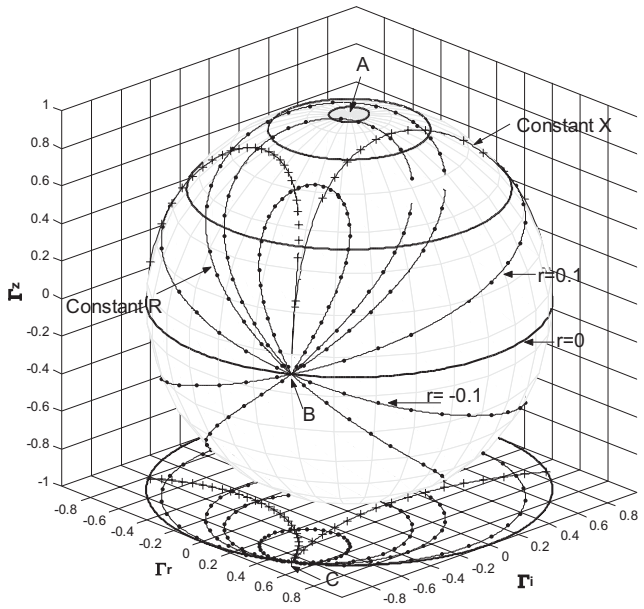

Figure 3 T-chart spherical representation ($\theta_1 = \pi/6$, $\theta_2 = -\pi/6$, $p = 1$,$|\Gamma|_{\max} = 1$)

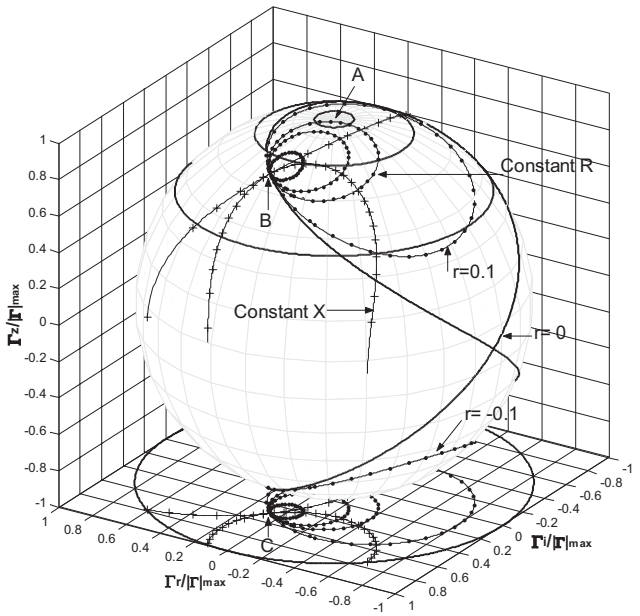

Figure 4 Omnipotent Smith chart spherical representation ($\theta_1 = -\pi/3$, $\theta_2 = \pi/8$, $p = 2$,$|\Gamma|_{\max} = 1.0016$)

its mapped point C on the $\Gamma_r - \Gamma_x$ plane, as most other points, have sharply changed its positions. As a matter of fact, from Figures 3 to 4, the original equator, namely the $r = 0$ constant resistance circle, has been twisted to keep its mapped curve on the $\Gamma_z = 0$ exactly the $r = 0$ circle in a 2D OSC. Because the $r = 0$ constant resistance circle always serves as the boundary between the positive region and the negative one, the former region shrinks and hence the latter expands. Those features make the spherical OSC much more complicated than the spherical standard Smith chart and spherical T-chart. Even so, the advantage that we expect is still obvious, that is to illustrate the passive and active components of RF devices explicitly on a single coordinate system without involving the infinite 2D plane. This is also the core concept of [8].

However, it is also interesting to emphasize that compared to the 3D coordinate system reported in [8], our system is advantageous in keeping the center of the constant reflection coefficient circles static (at the North Pole). From Figures 2–4, it can be seen that the constant resistance circle is distorted on the sphere surface, but it still keep its shape when mapped to the ($|\Gamma|_{\max} = 1$) plane.

5. CONCLUSION

In this article, the spherical representation of OSC is proposed. The mathematical expressions for a new spherical coordinate system are presented to plot the 3D OSC. This article is ready to provide the theory supported with the generalized Smith chart in spherical space. Besides, the 3D coordinate system established in this article can also be applied to the standard Smith chart and the generalized Smith chart. Further improvement and applications of spherical OSC will be discussed in the future.

ACKNOWLEDGMENTS

The authors express their gratitude to the financial support of National Natural Science Foundation of China (No. 60736002).

REFERENCES

1. W. Yongle, H. Haiyu, and L. Yuanan, An omnipotent Smith chart for lossy nonreciprocal transmission lines, Microwave Opt Technol Lett 49 (2007), 2392–2395.

2. W. Yongle, H. Haiyu, and L. Yuanan, An extended omnipotent Smith chart with active parameters, Microwave Opt Technol Lett, in press.
3. D.E. De Jersey, Imaginary Smith chart for evanescent-mode structures, Electron Lett 16 (1980), 93–94.
4. D. Torrungrueng and C. Thimaporn, A generalized zy smith chart for solving nonreciprocal uniform transmission-line problems, Microwave Opt Technol Lett 40 (2004), 57–61.
5. E. Gago-Ribas, C. Dehesa-Martinez, and M.J. Gonzalez-Morales, Complex analysis of the lossy-transmission line theory: A generalized Smith chart, Turk J Electr Eng Comput Sci 14 (2006), 173–194.
6. W. Yongle, L. Yuanan, and L. Shulan, Dynamic Smith chart based on lossy uniform transmission lines, Microelectronics (in Chinese) 37 (2007), 660–663.
7. D. Torrungrueng, P.Y. Chou, and M. Krairiksh, An extended zy t-chart for conjugately characteristic impedance transmission lines with active characteristic impedances, Microwave Opt Technol Lett 49 (2007), 1961–1964.
8. C. Zelley, A spherical representation of the Smith chart, IEEE Microwave Mag 8 (2007), 60–66.

A NOVEL HTS FILTER WITH IMPROVED OUT-OF-BAND REJECTION BY INTRODUCING A QUARTER-WAVELENGTH SPIRAL STUB

Yunlong Piao,[1] Xiaoping Zhang,[1] Xubo Guo,[1] Shichao Jin,[1] Bisong Cao,[1] Huili Peng,[1] Xinxiang Lu,[1] and Baoxin Gao[2]
[1] Department of Physics, Tsinghua University, Beijing 100084, People's Republic of China; Corresponding author: zhangxp@mail.tsinghua.edu.cn
[2] Department of Electrical Engineering, Tsinghua University, Beijing 100084, People's Republic of China

Received 23 January 2008

ABSTRACT: *A novel high temperature superconducting (HTS) filter with split-end stepped impedance resonators (SIR) is developed on MgO substrate. Spiral feedlines are used to meet the requirement of the external quality factor. A quarter-wavelength (λ/4) spiral stub is introduced at the input feedline to provide additional transmission zeros at the high frequency end, which can improve both the out-of-band rejection and band-edge steepness. The measured results at 70 K are in good agreement with the simulated ones.* © 2008 Wiley Periodicals, Inc.
Microwave Opt Technol Lett 50: 2455–2457, 2008; Published online in Wiley InterScience (www.interscience.wiley.com). DOI 10.1002/mop.23688

Key words: *HTS filter; stepped impedance resonator; spurious passband; out-of-band rejection; transmission zero*

1. INTRODUCTION

Since the discovery of high temperature superconducting (HTS) materials, HTS filters have attracted much attention for their promising applications in wireless communications, radar detection, and astronomical observation [1–4]. The extremely low surface resistance of HTS materials has enabled to realize the miniature thin-film filters with low insertion loss and high selectivity.

However, most HTS bandpass filters' developed with half-wavelength microstrip resonators, suffer from the inherent spurious passbands. Particularly, the nearest component is normally located at less than twice the fundamental frequency. In addition, this may lead to a degraded out-of-band rejection between the fundamental and first spurious passband. Therefore, it is desired to obtain a HTS filter with both wide stopband and high out-of-band rejection.

Quarter-wavelength resonator (QWR) has the advantage of spurious suppression, because its first spurious passband is located at three times the fundamental frequency [3]. However, one end of the QWR is required to be grounded, which is complicated for HTS materials and may degrade the resonator's Q factor. Recently, stepped impedance resonators (SIR) are reported to relocate the spurious passband [5, 6]. This structure has the advantages of compact size and avoiding grounding condition; its spurious passband can be relocated by adjusting the transmission lines' impedance ratio.

To obtain a good out-of-band rejection, the natural choice is to increase the pole number of filter or to add the cross coupling line [7]. But those may make filter design and fabrication complicated or increase the substrate size. Instead, some bandstop structures, such as notch and quarter-wavelength (λ/4) stub, can be incorporated into feedline to produce transmission zeros and improve the out-of-band rejection [8, 9].

In this article, we designed a 3-pole HTS bandpass filter using symmetrical split-end SIR to relocate the first spurious passband. Moreover, a λ/4 spiral stub is introduced at the input feedline of the filter to improve the out-of-band rejection between the fundamental and the first spurious passband.

2. FILTER DESIGN

2.1. Filter With the Split-End SIR

A novel 3-pole HTS bandpass filter with a 0.4% fractional bandwidth at 2993 MHz has been designed with the Split-end SIR, as shown in Figure 1(a). Spiral feedlines are used to increase the coupling between the spiral feedlines and the out-most resonators to meet the requirement of external quality factor.

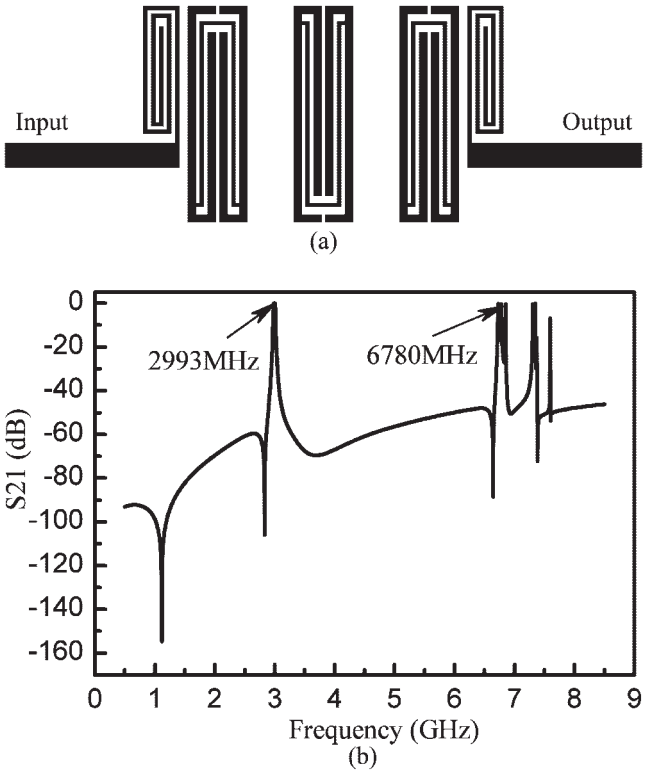

Figure 1 (a) Layout of the filter with split-end SIR. (b) The simulated wideband response of the filter